Report

Cell Reports

Structure of the Hantavirus Nucleoprotein Provides Insights into the Mechanism of RNA Encapsidation

Graphical Abstract

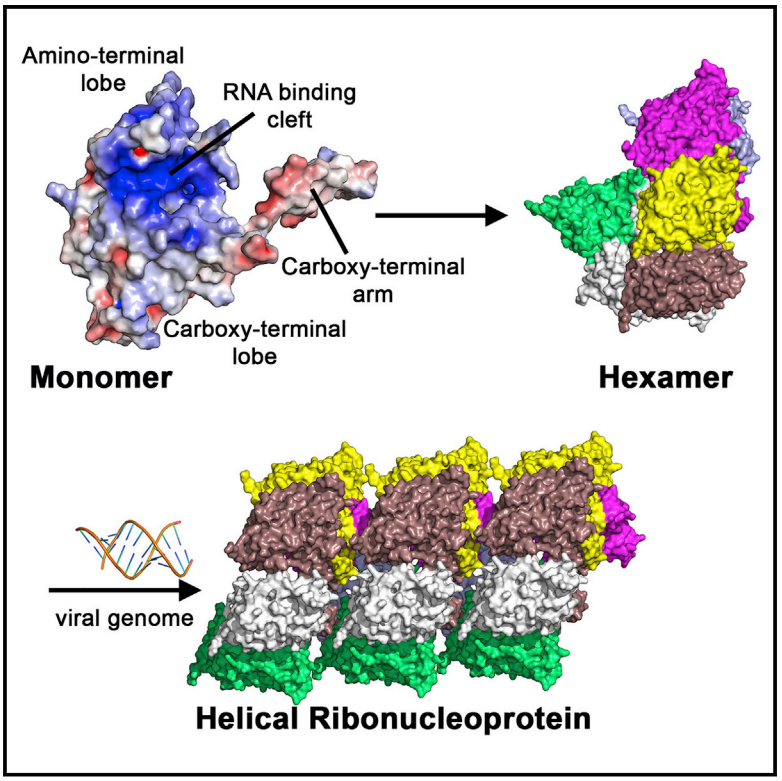

Authors

Daniel Olal, Oliver Daumke

Correspondence

daniel.olal@mdc-berlin.de (D.O.),
oliver.daumke@mdc-berlin.de (O.D.)

In Brief

Hantavirus is the causative agent of life-threatening hemorrhagic fever with renal syndrome. Olal and Daumke describe the crystal structure of the nucleoprotein of hantavirus and suggest a mechanism by which it oligomerizes and sequesters the viral RNA genome.

Highlights

- Hantavirus nucleoprotein shows a unique bilobed architecture
- The RNA binding site is located at the lobe intersection
- Oligomerization is mediated by amino- and carboxy-terminal arms

Accession Numbers

5FSG

Olal & Daumke, 2016, Cell Reports *14*, 2092–2099
March 8, 2016
http://dx.doi.org/10.1016/j.celrep.2016.02.005

CellPress

OPEN ACCESS
CellPress

Cell Reports
Report

Structure of the Hantavirus Nucleoprotein Provides Insights into the Mechanism of RNA Encapsidation

Daniel Olal[1,*] and Oliver Daumke[1,2,*]
[1]Crystallography, Max Delbrück Center for Molecular Medicine, Robert-Rössle-Strasse 10, 13125 Berlin, Germany
[2]Biochemie, Freie Universität Berlin, Takustrasse 6, 14195 Berlin, Germany
*Correspondence: daniel.olal@mdc-berlin.de (D.O.), oliver.daumke@mdc-berlin.de (O.D.)
http://dx.doi.org/10.1016/j.celrep.2016.02.005

SUMMARY

Hantaviruses are etiological agents of life-threatening hemorrhagic fever with renal syndrome and hantavirus cardiopulmonary syndrome. The nucleoprotein (N) of hantavirus is essential for viral transcription and replication, thus representing an attractive target for therapeutic intervention. We have determined the crystal structure of hantavirus N to 3.2 Å resolution. The structure reveals a two-lobed, mostly α-helical structure that is distantly related to that of orthobunyavirus Ns. A basic RNA binding pocket is located at the intersection between the two lobes. We provide evidence that oligomerization is mediated by amino- and C-terminal arms that bind to the adjacent monomers. Based on these findings, we suggest a model for the oligomeric ribonucleoprotein (RNP) complex. Our structure provides mechanistic insights into RNA encapsidation in the genus *Hantavirus* and constitutes a template for drug discovery efforts aimed at combating hantavirus infections.

INTRODUCTION

Hantaviruses are single-stranded negative-sense RNA bunyaviruses that mostly replicate in rodents, often without causing disease (Jonsson et al., 2010). In humans, hantavirus infections can lead to potentially fatal hemorrhagic fever with renal syndrome (HFRS) and hantavirus cardiopulmonary syndrome (HCPS), for which no specific cure is available to date. HFRS is caused by Old World hantaviruses like Hantaan virus (HTNV). New World hantaviruses like Sin Nombre virus (SNV) are responsible for the more severe HCPS.

The large (L) segment of the tripartite genome of hantavirus encodes the viral-RNA-dependent RNA polymerase (RdRp) whereas the medium (M) and small (S) segments encode the spike glycoproteins (called Gn and Gc), and the nucleoprotein (N) and nonstructural (NS) proteins, respectively (Schmaljohn, 1995). The transcriptase and replicase functions of the virus reside in the ribonucleoprotein (RNP) complex, which comprises the viral RdRp, N, and the viral RNA. Multiple pleiotropic functions of N, such as in immune evasion, have previously been demonstrated (Taylor et al., 2009). More recently, N was shown to play a crucial role in ''cap snatching'' through the sequestration of cellular 5′ RNA caps in P bodies, thus enabling viral transcriptional regulation (Hussein and Mir, 2013). Furthermore, N can functionally replace components of the eukaryotic eIF4F cap binding complex to link the mRNA cap with the 43S pre-initiation complex, therefore guaranteeing preferential translation of viral RNA.

Recent studies have explored N structures of various bunyaviruses. Thus, representative N structures of orthobunyaviruses, such as LaCrosse (Reguera et al., 2013), Bunyamwera (Li et al., 2013), Leanyer (Niu et al., 2013), and Schmallenberg virus (Dong et al., 2013); of phleboviruses, such as Rift Valley fever (Raymond et al., 2012) and Toscana virus (Olal et al., 2014; Raymond et al., 2012); and of nairoviruses, such as Crimean-Congo hemorrhagic fever virus (Guo et al., 2012), have been determined. Within each bunyavirus genus, the N structures are highly similar. Between the various genera, however, only little structural similarity is apparent, in agreement with the missing sequence similarity between these Ns: All bunyavirus Ns have a bilobed, α-helical architecture. While orthobunyaviruses employ amino- and C-terminal arms for N oligomerization, an amino-terminal arm suffices for N oligomerization of phleboviruses. Hantavirus Ns bear no detectable sequence similarity with the Ns of other genera or family. The structures of the 71-amino-acid N-terminal domain of Sin Nombre and Andes hantaviruses show two antiparallel helices that intertwine to form a coiled coil and may contribute to oligomerization (Boudko et al., 2007).

The intrinsic flexibility of N and its propensity to oligomerize into polymers at high concentrations has hampered its structural characterization. We addressed this challenge by crystallizing a HTNV N construct fused to a maltose binding protein (MBP). The crystal structure of this construct reveals a unique architecture of HTNV Ns and provides a framework for understanding its mechanism of RNA sequestration and oligomerization. Furthermore, the structure offers a template for rational drug design efforts aimed at combating hantavirus infections.

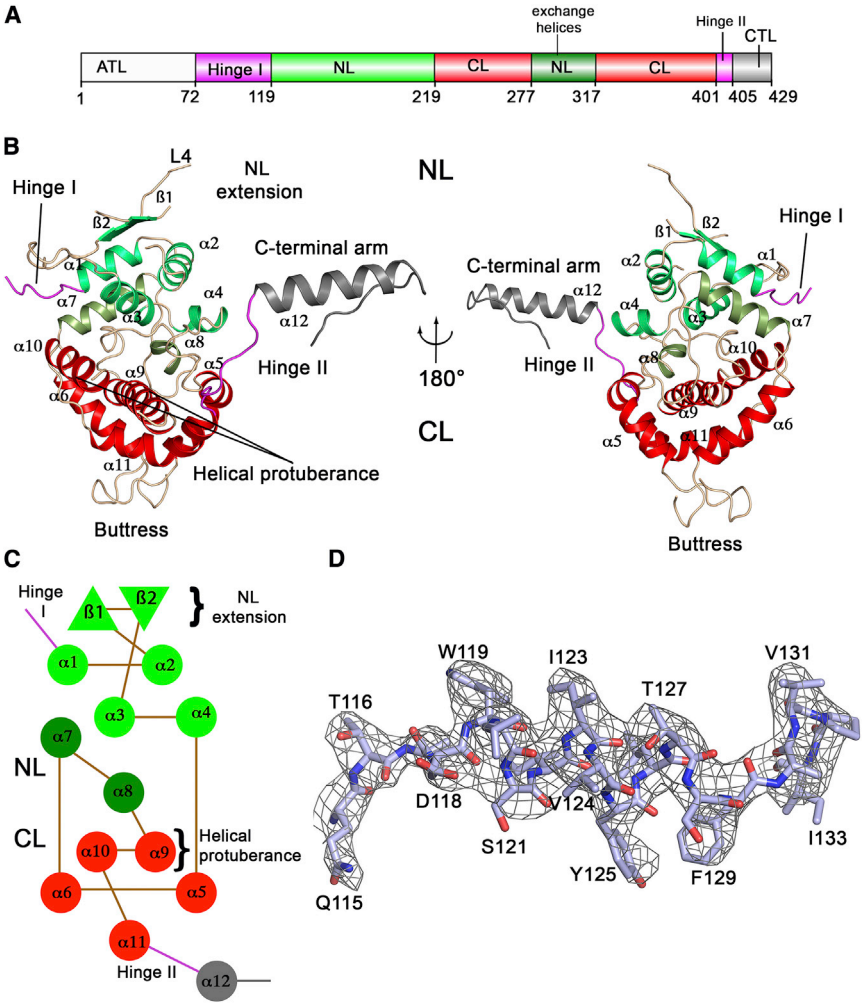

Figure 1. Structure of the HTNV N

(A) Domain organization of HTNV N. ATL, amino-terminal arm; CTL, carboxy-terminal arm.

(B) Structure of the HTNV $N^{\Delta N}$ showing a bilobed core domain and the C-terminal arm.

(C) Topology plot of the HTNV $N^{\Delta N}$. α helices are shown as circles and β strand as triangles, with colors as in (A).

(D) Representative refined electron densities of $HTNV^{\Delta N}$ N around helix α1, contoured at 1 σ.

See also Figure S1 and Tables S1–S3.

RESULTS

Structure of the HTNV N

To obtain structural and mechanistic insights into RNA encapsidation in the hantavirus family, we crystallized a HTNV N construct containing an amino-terminal deletion (residues 113–429, HTNV $N^{\Delta N}$) fused to MBP and collected diffraction data to 3.2 Å (Table S1). The phase problem was solved by molecular replacement using MBP (Table S1).

HTNV $N^{\Delta N}$ is a mostly α-helical protein composed of an amino-terminal lobe (NL; residues 119–218 and 277–316) and a C-terminal lobe (CL; residues 219–276 and 317-400) (Figure 1; Table S2). Together, they form the N core (residues 119–400), from which an α-helical extension projects away (residues 401-429). The NL comprises an α-helical bundle formed by helices α1–α4. In addition, helix α7 crosses over from the CL and participates in the helical assembly of the NL, whereas α8 locates in between the two lobes (Figures 1B and 1C). Two antiparallel β strands, β1 and β2, and the intervening loop L4 form an extension of the NL that connects α2 to α3. Parts of this extension are disordered, whereas other parts are stabilized by crystal contacts from the adjacent MBP molecule. The amino-terminal arm (residues 1–119), which is mostly missing in our construct, contains the previously crystallized coiled-coil domain (residues 1–71; Figure S1A) (Boudko et al., 2007). It is connected to the NL via a predicted hinge (hinge I, residues 72–118), of which only the C-terminal portion is present in our structure.

The CL comprises helices α5, α6, and α9–α11. α5 and α6 are linked by a 22-residue loop, L8, that bulges 13 Å out from the bottom of the CL. Hydrophobic residues make up half of this partially disordered loop, suggesting that it may act as a binding platform or buttress (see below). α9 and α10 form a mast-like helical protuberance that abuts 38 Å from the core structure (Figure 1B). At the C terminus, a helical arm (residues 405–429) extends from the CL (Figures 1B and 1C). It is connected to the globular core via a flexible hinge region (hinge II, residues 401–404) and binds into a hydrophobic pocket of the adjacent molecule (see below).

Hantavirus N does not have significant sequence similarity to Ns of other bunyaviruses. However, we found a distant structural relationship to the Ns of orthobunyaviruses (Leanyer/LEAV, LaCrosse, and Schmallenberg virus) and phleboviruses (Rift Valley fever and Toscana virus) (Figures S1A–S1F; Table S3) (Niu et al., 2013; Olal et al., 2014). Intriguingly, also the N of Lassa virus (Hastie et al., 2011), an Arenavirus, bears weak similarity to HTNV N (Table S3).

Despite the much shorter size of the LEAV N compared to HTNV N (235 versus 429 amino acids for the full-length N), some structural elements in the NL, including β1 and β2, and helices α1–α4 are conserved between the structures (Table S3; Figures S1A–S1D). However, marked differences are prevailing: The "exchange helix" α7 in HTNV N does not have a counterpart in LEAV N. Furthermore, the amino-terminal arm containing the coiled coil and hinge I has 118 residues in HTNV N and only 20 residues in LEAV N (Figure S1A) (Boudko et al., 2007). In fact, hinge I in HTNV N may represent an independent functional domain, since this region has been shown to encompass the

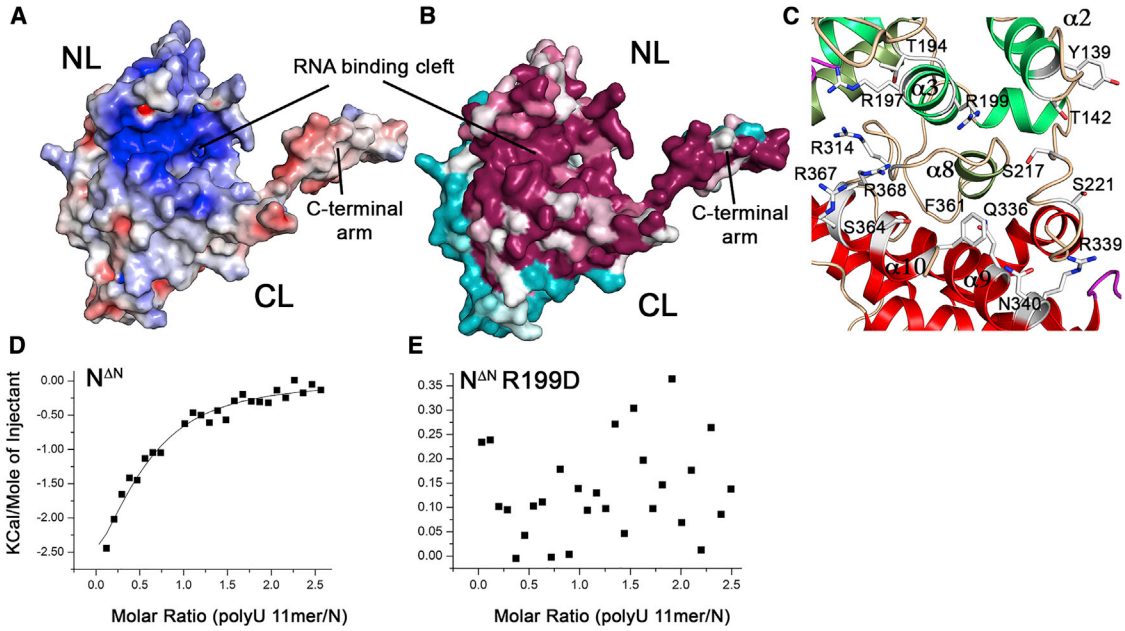

Figure 2. The RNA Binding Groove of HTNV N

(A) Electrostatic surface representation (±5 kT) of HTNV $N^{\Delta N}$ in a similar orientation as in Figure 1B, left. Positive and negatively charged surfaces are colored in blue and red, respectively. A highly basic RNA binding groove is apparent in between the two lobes.

(B) Surface representation of HTNV $N^{\Delta N}$ in the same orientation as in Figure 2A, colored according to evolutionary conservation (for the alignment, see Table S2). Brown and cyan indicate conserved through variable surface-exposed residues.

(C) Cartoon representation showing select residues of HTNV $N^{\Delta N}$ in the predicted RNA binding tunnel between the NL (green) and CL (red).

(D) ITC binding curve of the 11-mer poly U RNA oligo1: MBP-HTNV $N^{\Delta N}$ (K_D = 11.1 μM ± 1.4 μM, n = 0.5).

(E) The MBP-HTNV $N^{\Delta N}$ R199D mutant did not show binding to RNA in ITC experiments.

See also Figure S2.

RPS19 binding site in HTNV N (Ganaie et al., 2014). The differences in the CLs between these two Ns are even more pronounced. Helices α6, α9, and α10 in LEAV N do not have equivalents in HTNV N. Conversely, the buttress (loop L8) is unique to hantaviruses. This loop is also the most variable region within hantavirus N. The helical protuberance (α9–α10, 50 residues) of HTNV N has double the size compared to LEAV N (α11–α12, 25 residues). Also, the C-terminal arm of HTNV N is twice as long as that of the orthobunyavirus counterpart (29 versus 15 residues). The differences between HTNV N and phlebovirus N are even more conspicuous. The NL extension of phleboviruses is mainly composed of α helices and thus has a different architecture compared to that of hantaviruses (Figures S1E and S1F). In the CL, α11 and α14 do not bear equivalents in HTNV N. Also the helical protuberance is greatly diminished in size in phleboviruses. However, the starkest difference is the loss of the C-terminal arm in phleboviruses. Taken together, these results suggest that Ns of hanta-, orthobunya, and phleboviruses arose from a common progenitor, yet they considerably diverged during evolution.

Interestingly, we found that the CL of HTNV N shares structural similarity with the two MA3 domains of the non-viral, eukaryotic tumor suppressor protein programmed cell death 4 (PDCD4) (Figures S1G and S1H; Table S3). In particular, helices α8–α12 of HTNV N were found to superimpose with the corresponding counterparts in the MA3 domains.

RNA Binding

HTNV Ns differentially interact with viral mRNA, genomic viral RNA (vRNA), and complementary RNA (cRNA) (Severson et al., 2001). To map the RNA binding site, we calculated the electrostatic surface potential of N (Figure 2A). A positively charged cleft formed by α3 and α4 of the NL and α9 and α10 of the CL was identified as a putative RNA binding interface. This groove is highly conserved across all hantavirus species (Figures 2B and 2C).

The purified amino-terminal truncated HTNV N had an optical density 260 (OD_{260})/OD_{280} ratio of 0.6, suggesting that it was free of nucleic acids. Accordingly, in isothermal titration calorimetry (ITC) experiments, MBP-HTNV $N^{\Delta N}$ bound to 11- and 14-mer polyU RNA with modest affinity (K_D of ~10 μM; Figures 2D and S2A–S2C). To confirm the putative RNA binding site, the surface-exposed conserved Arg199 in this region was mutated to aspartate. Indeed, the R199D substitution within the MBP-HTNV $N^{\Delta N}$ construct completely abrogated the interaction with RNA (Figure 2E). Two regions in the NL termed N1 (residues 175–196) and N2 (residues 197–218) were previously shown to contain RNA binding residues (Figures S2D and S2E) (Xu et al., 2002). Our structure shows that N1 residues Ser180, Asn183, Ser186, Ser187, and Thr194 line the deduced RNA binding groove and could form hydrogen bonds to the RNA bases or the phosphate backbone. In addition, the positively charged Lys189, Arg197, and Arg199 from N2 could

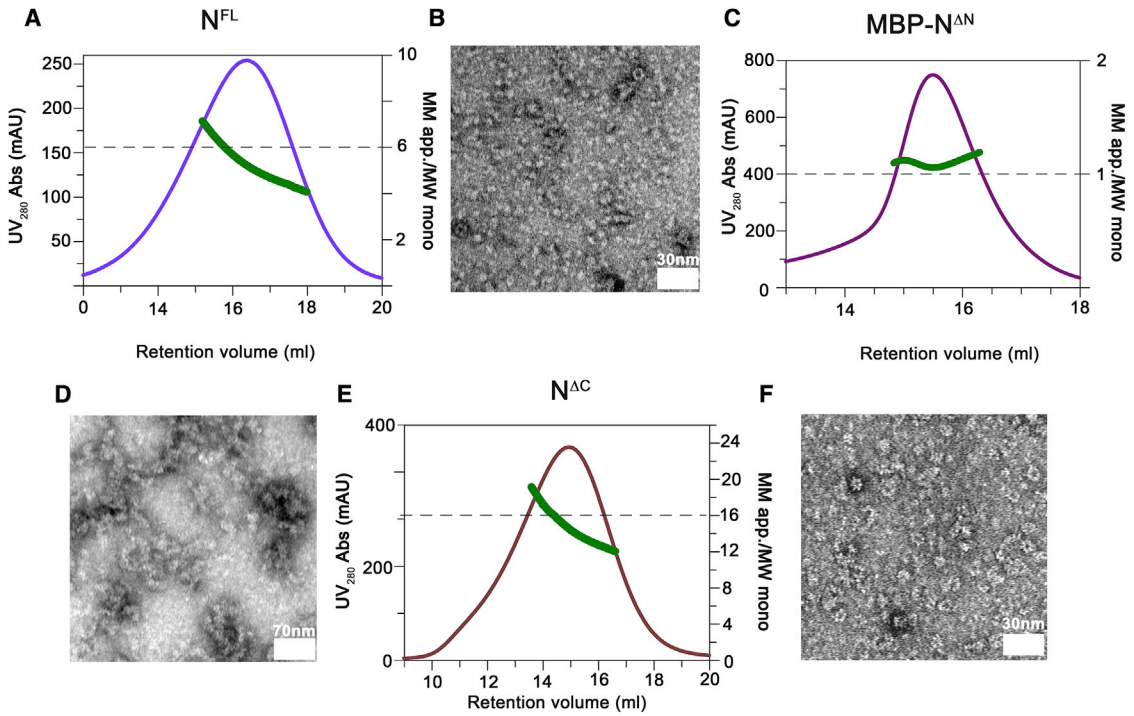

Figure 3. Oligomerization Studies of the HTNV N

(A) Gel filtration analysis (Superose 6 10/300) coupled to RALS of full-length refolded HTNV N. UV absorbance is shown in violet and refers to the left y axis, while the apparent molecular mass (in multiples of the molecular weight of the monomer) is shown in green and refers to the right y axis.

(B) Negative stain EM of refolded full-length HTNV N in the absence of RNA.

(C) Gel filtration analysis (Superdex S200 10/300) coupled to RALS of the monomeric MBP-HTNV $N^{\Delta N}$.

(D) Negative-stain EM of chimeric MBP-HTNV $N^{\Delta N}$ incubated with an 8 kb ssRNA.

(E) Gel filtration analysis (Superose 6 10/300) coupled to RALS of HTNV $N^{\Delta C}$.

(F) Negative-stain EM of HTNV $N^{\Delta C}$ in the absence of RNA.

See also Figures S3 and S4.

form salt bridges with the phosphate backbone (Figure S2D). Also residues 335-429 were suggested to be involved in RNA binding (Figure S2E) (Gött et al., 1993). This region encompasses the helical protuberance (α9 and α10) in the CL and the C-terminal arm. Our structure shows that residues of the helical protuberance, including Arg339 (α9), Arg367, and Arg368 (both α10), may indeed project into the RNA binding cleft to neutralize the charge of the RNA phosphate groups. Furthermore, the highly basic disordered loop L12 between α9 and α10 could contribute to nucleic acid stabilization. Taken together, our data suggest that residues in between the NL and CL, and possibly in the hinge regions, constitute a highly conserved RNA binding site in HTNV Ns.

Oligomerization of HTNV N

Previous biochemical data indicated essential roles of amino- and C-terminal regions in HTNV N for oligomerization (Alfadhli et al., 2001). In particular, residues 100–125 in the amino-terminal arm and residues 404–429 in the C-terminal arm were implicated in this process (Yoshimatsu et al., 2003). Furthermore, a conserved hexapeptide motif preceding the C-terminal arm (393-VNHFHL-398) (Figure S3A) was suggested to be involved in the multimerization of Tula hantavirus N (Kaukinen et al., 2003).

To further study the mechanism of oligomerization, we purified and refolded full-length HTNV N. Right-angle laser scattering analysis (RALS) in conjunction with analytical size-exclusion chromatography (SEC) indicated that HTNV N exists mostly as a hexamer in solution (Figure 3A), rather than as trimer, as reported earlier (Hussein and Mir, 2013). In negative-stain electron microscopy (EM), HTNV N formed toroidal rings with a diameter of 10–13 nm (Figures 3B and S4). In contrast, MBP-HTNV $N^{\Delta N}$ eluted as a monomer under identical conditions (Figure 3C). This supports the suggested role of the amino-terminal arm for oligomerization in HTNV Ns.

In the presence of a long ssRNA, MBP-HTNV $N^{\Delta N}$ assembled into long filaments, as visualized by EM (Figure 3D). Thus, even in the absence of the amino-terminal arm, MBP-HTNV $N^{\Delta N}$ can bind in some regular fashion around an RNA template. In contrast, the RNA-binding-deficient R199D mutant assembled into amorphous supercoiled structures that were distinct from the HTNV RNP filaments (Figure S4). These experiments point to a coupling of RNA binding and oligomerization.

Surprisingly, a structure-based construct devoid of the entire C-terminal arm (HTNV $N^{\Delta C}$) eluted as a high-molecular-weight oligomer with an apparent molecular mass >700 kDa in SEC

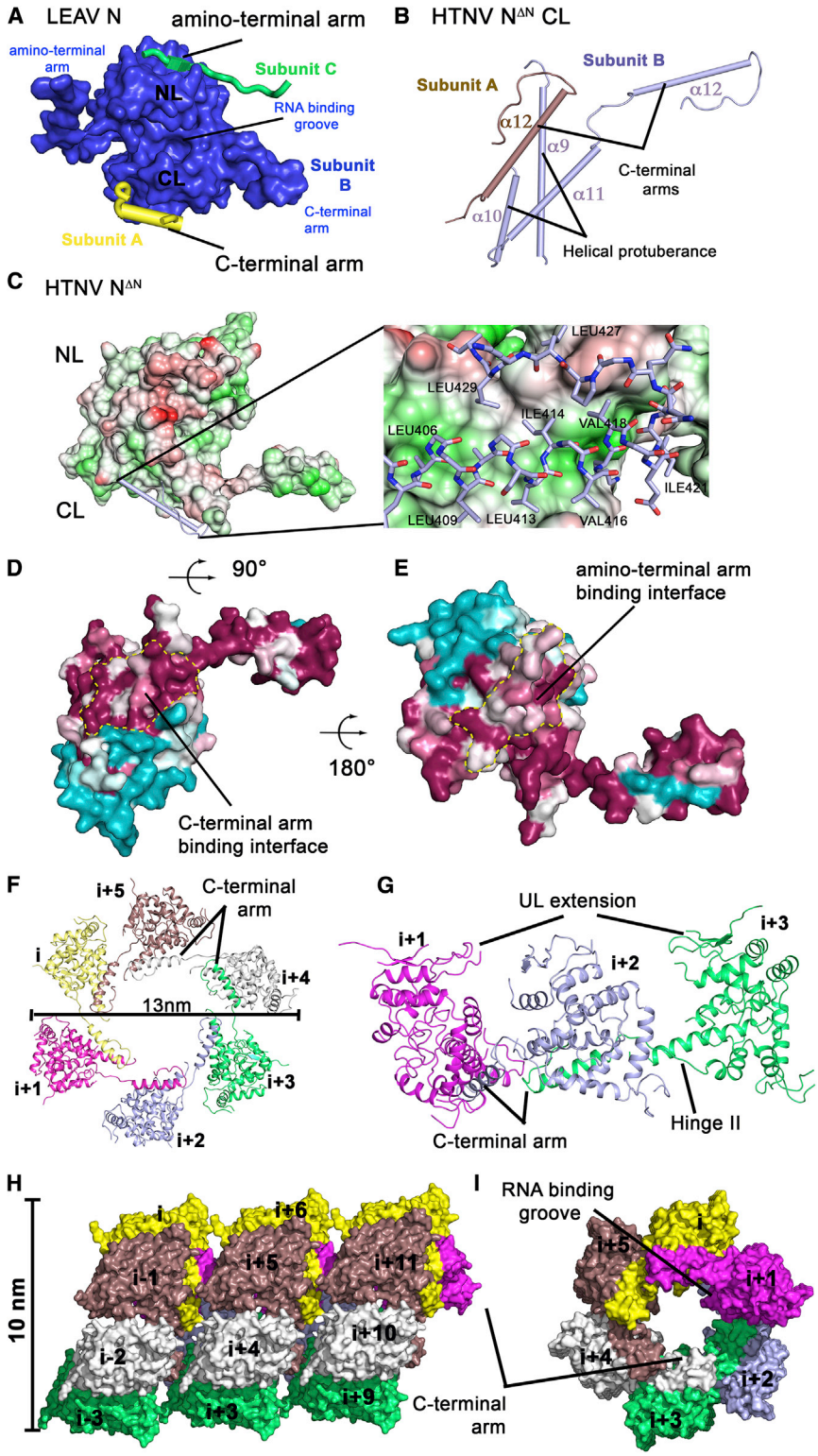

Figure 4. Structural Determinants of Oligomerization in Hantavirus N

(A) Surface representation of one LEAV N subunit within the tetramer (molecule B, PDB: 4J1G) showing opposite binding interfaces for the amino- and C-terminal arms of two flanking subunits (from molecule A to the left and molecule C to the right).

(B) Cartoon representation of the HTNV N CL (light blue). The C-terminal arm of the adjacent molecule (brown) binds into a similar pocket as in LEAV N, close to the helical protuberance.

(C) Hydrophobic surface representation showing interaction details of the C-terminal arm in HTNV N. Hydrophobic and polar residues are shown in green and red, respectively. The orientation corresponds to that of LEAV N in Figure 4A.

(D) Surface conservation plots of the HTNV $N^{\Delta N}$ LL (view on the CL) showing that the binding groove for the C-terminal arm is conserved in hantaviruses. Conserved residues are shown in maroon, whereas non-conserved residues are shown in cyan. The orientation relative to (C) is indicated by the arrow.

(E) Surface conservation plots of HTNV $N^{\Delta N}$ UL (view along the NL) showing the predicted, highly conserved binding groove for the amino-terminal arm. The orientation relative to (D) is indicated by an arrow.

(F) Ribbon representation of a hexameric HTNV N model showing how the C-terminal arms could mediate the assembly.

(G) Side view of (F).

(H) Side view on a left-handed helical model of the HTNV RNP, based on a related model of Toscana virus RNP.

(I) Top view of this helix. The RNA binding site is located in a continuous groove in the interior of the RNP.

See also Figures S3 and S4.

(Figure 3E). EM micrographs of the negatively stained HTNV $N^{\Delta C}$ samples showed toroidal assemblies that range from compact regular hexamers to larger amorphous rings (Figure 3F). Thus, in the presence of the amino-terminal arm, the C-terminal arm may regulate the oligomerization process.

A comparison of the HTNV and LEAV N structures suggested that the oligomerization mechanism may be related in these two N families (Figure 4). In the RNA-bound LEAV tetramer, the C-terminal arm of the first subunit binds into a hydrophobic pocket of the CL in the adjacent subunit (Figure 4A). Also in our HTNV N structure, the C-terminal arm binds to a similar surface-exposed groove of an adjacent N in the crystals (Figure 4B). In contrast to LEAV, this assembly results not in the formation of a closed tetramer but in a linear N oligomer in the crystal lattice (Figure S3B). The exchanged arm buries a surface area of 860 $Å^2$, primarily via hydrophobic contacts (Figure 4C). The binding groove of the C-terminal arm in HTNV N includes the helical protuberance and α11 in the CL

(Figures 4B and 4C) and is highly conserved between hantaviruses (Figure 4D). In agreement with these observations, residues 340–379 partially constituting the hydrophobic groove were previously shown to be required for N-N interactions (Kaukinen et al., 2003). In addition to the C-terminal arm, the amino-terminal arm of LEAV N binds into a polar pocket of the second adjacent N (Figure 4A). The equivalent surface in the NL of HTNV N includes residues of β1, β2, and the intervening loop L4 and is highly conserved among different hantavirus species (Figure 4E).

HTNV $N^{\Delta N}$ polymerizes around its tripartite genome forming helical RNPs that have a diameter of ~10 nm (Figure 3D) (Battisti et al., 2011). On the evidence of our RALS, EM and structural data, we modeled a hexameric HTNV N assembly with a diameter of ~10 nm using the helical model of the related Toscana virus RNP as a template (Figures 4F–4I) (Olal et al., 2014). In this HTNV model, the C-terminal arm binds into the hydrophobic groove of the CL in the adjacent subunit (i+1; Figures 4F and 4G). Furthermore, the amino-terminal coiled-coil domain would be in close apposition to the conserved surface in the NL of the previous (i−1) subunit (Figure 4E) and may bind to this surface. Similarly as previously suggested for Toscana virus RNPs, long RNA sequences could be incorporated in a continuous RNA binding groove in the interior of the N helix (Figures 4H and 4I).

DISCUSSION

Phylogenetic analyses in *Bunyaviridae* have mainly been based on sequence comparisons of the RNA polymerase, which is the most highly conserved protein in this family (Marklewitz et al., 2015). In contrast, N sequences could not be employed for phylogenetic comparisons, due to their low degree of sequence similarity. The degree of structural similarity of HTNV N was highest for orthobunyavirus N, decreased for Phlebovirus, and decreased even further for arenavirus Ns. No structural similarity was found for the Ns of nairoviruses. Not only the structure but also the assembly mode of hantavirus Ns via amino- and/or C-terminal arms appears to be related to that of orthobunyavirus Ns. These results are in close agreement with the phylogenetic relations deduced from RNA polymerase sequence analyses (Marklewitz et al., 2015). They demonstrate the versatility of structural comparisons for phylogenetic analyses, when sequence conservation is sparse (Marsh and Teichmann, 2015).

In eukaryotes, HTNV N is most closely related to the two MA3 domains of the tumor suppressor PDCD4. Both M3 domains of PDCD4 were shown to bind to the translation initiation factor eIF4A (Chang et al., 2009), an ATP-dependent RNA helicase, which interacts with the scaffold protein eIF4G and the cap-binding protein eIF4E to form the eIF4F complex. PDCD4 was shown to block the interaction of eIF4A with eIF4G, resulting in the suppression of cap-dependent translation. Interestingly, HTNV N was shown to substitute for the entire eIF4F function resulting in the preferential translation of viral RNAs (Hussein and Mir, 2013). Our structural studies raise the interesting possibility that HTNV N structurally mimics PDCD4 to promote translation of viral mRNAs or to actively repress translation of host mRNA.

We identified a basic RNA binding cleft between the NL and CL. In particular, residues of the helical protuberance, of L12 and of the two hinge regions may be involved in RNA binding. The location of the RNA binding groove between the two lobes, at the inside of the N oligomer, is similar to that of other bunyavirus Ns. Like most viruses, hantaviruses lack mRNA capping machinery. An endonuclease function encoded by the viral RdRp typically cleaves host mRNA and uses the capped substrates as primers in a process termed "cap snatching" (Hussein and Mir, 2013). Also HTNV N was suggested to harbor an m7 G cap-binding site (CBS) that is distinct from the RBD (Hussein and Mir, 2013). In our HTNV N structure, however, we did not find evidence for a conserved CBS with basic or aromatic clusters on the surface of the protein (Mazza et al., 2001). Thus, it is currently unclear whether such CBS exists in HTNV N and if, where it may be located.

Also the oligomerization mode of HTNV and orthobunyavirus Ns appears related. It entails the insertion of a C-terminal arm of the N_i protomer into the core domain of the N_{i+1} subunit. In agreement with such model, our data indicate that the C-terminal arm of HTNV N regulates the assembly of N into a regular oligomer. A similar role may be envisaged for the amino-terminal arm, which is crucial for the hexameric assembly of HTNV N. Similar to LEAV, it may bind to the related, highly conserved surface of the NL in N_{i-1} subunit. Interestingly, both hinge regions of LEAV N were shown to directly contribute to RNA binding (Niu et al., 2013), and we envisage that similar contacts with the RNA base may occur in HTNV N. Via these contacts, RNA binding could be coupled to oligomerization, allowing a concerted mechanism of RNA encapsidation. In agreement with such hypothesis, a yeast two-hybrid assay identified the invariant Trp119 in hinge I in the Seoul hantavirus as crucial determinant for N assembly (Yoshimatsu et al., 2003). In our RNA-free structure, Trp119 interacts with Arg197 in α3 via cation-π stacking (Figure S3C) and may allow the proper folding of hinge I as a prerequisite for assembly.

Crystal structures of negative-strand RNA virus nucleocapsid proteins interacting with RNA were initially reported for the non-segmented *Rhabdoviridae* (Albertini et al., 2006; Green et al., 2006). Similar oligomerization and RNA interactions modes between two lobes, as suggested here for the HTNV N, were identified. Helical reconstructions of respiratory-syncytial-virus (RSV) RNP showed a left-handed helix with a pitch of 68–100 Å and 10–11 subunits per turn (Bakker et al., 2013; Tawar et al., 2009). In contrast, Sendai and measles virus RNPs exist in multiple conformations that have a shorter pitch ranging from 52–68 Å corresponding to ~13 N subunits per turn (Egelman et al., 1989; Maclellan et al., 2007). Toscana virus RNP crystallized as a staggered hexamer, which provides the basis for a helical model of RNPs assembly in phleboviruses (Olal et al., 2014). Based on this model, we suggest an analogous helical model for the HTNV RNP. The dimensions of our RNP model (10 nm diameter) are in agreement with the dimensions of the RNP observed by EM analyses (Battisti et al., 2011).

Our analyses identified three unique, highly conserved surfaces in the HTNV N that correspond to the predicted binding pocket of the amino-terminal coiled coil in the NL, the binding pocket of the C-terminal arm in the CL, and the RNA binding cleft. Small molecules that bind into these pockets with high affinity would likely interfere with RNA binding and/or

oligomerization and therefore block viral replication, similar to related drugs targeting the nucleoproteins of RSV and influenza viruses (Challa et al., 2015; Kao et al., 2010). In such way, the HTNV N structure can guide structure-based drug design efforts aimed at developing anti-hantavirus compounds.

EXPERIMENTAL PROCEDURES

Expression and Crystallization

His-tagged full-length (1–429) or C-terminally truncated (1–401) HTNV N in the pET46 vector and MBP-tagged HTNV N (113–429) in the pET21 vector were expressed in *E. coli* and purified via standard procedures (see also Supplemental Experimental Procedures). MBP-HTNV $N^{\Delta N}$ crystallized in 17%–20% PEG3350 and 0.2 M ammonium citrate (pH 5.0–5.5).

Data Collection and Structure Determination

Diffraction data of single crystals were collected at BESSY-II BL14.1 and DESY BL P11. The structure was determined by molecular replacement. DALI was used for structural comparisons (Holm and Rosenström, 2010).

Electron Microscopy

1.5 mg/ml protein and an 8,000-base ssRNA were mixed and diluted 10-fold. 15 μl of the sample was spotted on carbon-coated grids stained with 2% uranyl acetate.

ITC

Experiments were carried out at 15°C using stepwise titrations of a 400-μM RNA solution into a 25-μM protein solution in the reaction cell.

ACCESSION NUMBERS

The accession number for the coordinates and structure factors for the HTNV N is PDB: 5FSG.

SUPPLEMENTAL INFORMATION

Supplemental Information includes Supplemental Experimental Procedures, four figures, and three tables can be found with this article online at http://dx.doi.org/10.1016/j.celrep.2016.02.005.

AUTHOR CONTRIBUTIONS

D.O. conducted the experiments. D.O. and O.D. designed the experiments, analyzed data, and wrote the manuscript.

ACKNOWLEDGMENTS

This work was supported by a German Research Foundation grant (DFG DA 1127/1 to O.D.). We thank M. Raftery (Charité) for providing the HTNV N plasmid. We are grateful to U. Müller, M. Weiss (both BESSY), A. Burkhardt, and S. Panneerselvam (both DESY) for beamline assistance and B. Purfürst for EM assistance. We also thank G. Kochs for helpful discussions as well as V. Schulz, A. Xavier, and J. Trzmiel for practical assistance.

Received: October 20, 2015
Revised: December 7, 2015
Accepted: January 25, 2016
Published: February 25, 2016

REFERENCES

Albertini, A.A., Wernimont, A.K., Muziol, T., Ravelli, R.B., Clapier, C.R., Schoehn, G., Weissenhorn, W., and Ruigrok, R.W. (2006). Crystal structure of the rabies virus nucleoprotein-RNA complex. Science *313*, 360–363.

Alfadhli, A., Love, Z., Arvidson, B., Seeds, J., Willey, J., and Barklis, E. (2001). Hantavirus nucleocapsid protein oligomerization. J. Virol. *75*, 2019–2023.

Bakker, S.E., Duquerroy, S., Galloux, M., Loney, C., Conner, E., Eléouët, J.F., Rey, F.A., and Bhella, D. (2013). The respiratory syncytial virus nucleoprotein-RNA complex forms a left-handed helical nucleocapsid. J. Gen. Virol. *94*, 1734–1738.

Battisti, A.J., Chu, Y.K., Chipman, P.R., Kaufmann, B., Jonsson, C.B., and Rossmann, M.G. (2011). Structural studies of Hantaan virus. J. Virol. *85*, 835–841.

Boudko, S.P., Kuhn, R.J., and Rossmann, M.G. (2007). The coiled-coil domain structure of the Sin Nombre virus nucleocapsid protein. J. Mol. Biol. *366*, 1538–1544.

Challa, S., Scott, A.D., Yuzhakov, O., Zhou, Y., Tiong-Yip, C.L., Gao, N., Thresher, J., and Yu, Q. (2015). Mechanism of action for respiratory syncytial virus inhibitor RSV604. Antimicrob. Agents Chemother. *59*, 1080–1087.

Chang, J.H., Cho, Y.H., Sohn, S.Y., Choi, J.M., Kim, A., Kim, Y.C., Jang, S.K., and Cho, Y. (2009). Crystal structure of the eIF4A-PDCD4 complex. Proc. Natl. Acad. Sci. USA *106*, 3148–3153.

Dong, H., Li, P., Böttcher, B., Elliott, R.M., and Dong, C. (2013). Crystal structure of Schmallenberg orthobunyavirus nucleoprotein-RNA complex reveals a novel RNA sequestration mechanism. RNA *19*, 1129–1136.

Egelman, E.H., Wu, S.S., Amrein, M., Portner, A., and Murti, G. (1989). The Sendai virus nucleocapsid exists in at least four different helical states. J. Virol. *63*, 2233–2243.

Ganaie, S.S., Haque, A., Cheng, E., Bonny, T.S., Salim, N.N., and Mir, M.A. (2014). Ribosomal protein S19-binding domain provides insights into hantavirus nucleocapsid protein-mediated translation initiation mechanism. Biochem. J. *464*, 109–121.

Gött, P., Stohwasser, R., Schnitzler, P., Darai, G., and Bautz, E.K. (1993). RNA binding of recombinant nucleocapsid proteins of hantaviruses. Virology *194*, 332–337.

Green, T.J., Zhang, X., Wertz, G.W., and Luo, M. (2006). Structure of the vesicular stomatitis virus nucleoprotein-RNA complex. Science *313*, 357–360.

Guo, Y., Wang, W., Ji, W., Deng, M., Sun, Y., Zhou, H., Yang, C., Deng, F., Wang, H., Hu, Z., et al. (2012). Crimean-Congo hemorrhagic fever virus nucleoprotein reveals endonuclease activity in bunyaviruses. Proc. Natl. Acad. Sci. USA *109*, 5046–5051.

Hastie, K.M., Liu, T., Li, S., King, L.B., Ngo, N., Zandonatti, M.A., Woods, V.L., Jr., de la Torre, J.C., and Saphire, E.O. (2011). Crystal structure of the Lassa virus nucleoprotein-RNA complex reveals a gating mechanism for RNA binding. Proc. Natl. Acad. Sci. USA *108*, 19365–19370.

Holm, L., and Rosenström, P. (2010). Dali server: conservation mapping in 3D. Nucleic Acids Res. *38*, W545–W549.

Hussein, I.T., and Mir, M.A. (2013). How hantaviruses modulate cellular pathways for efficient replication? Front. Biosci. (Elite) *5*, 154–166.

Jonsson, C.B., Figueiredo, L.T., and Vapalahti, O. (2010). A global perspective on hantavirus ecology, epidemiology, and disease. Clin. Microbiol. Rev. *23*, 412–441.

Kao, R.Y., Yang, D., Lau, L.S., Tsui, W.H., Hu, L., Dai, J., Chan, M.P., Chan, C.M., Wang, P., Zheng, B.J., et al. (2010). Identification of influenza A nucleoprotein as an antiviral target. Nat. Biotechnol. *28*, 600–605.

Kaukinen, P., Vaheri, A., and Plyusnin, A. (2003). Mapping of the regions involved in homotypic interactions of Tula hantavirus N protein. J. Virol. *77*, 10910–10916.

Li, B., Wang, Q., Pan, X., Fernández de Castro, I., Sun, Y., Guo, Y., Tao, X., Risco, C., Sui, S.F., and Lou, Z. (2013). Bunyamwera virus possesses a distinct nucleocapsid protein to facilitate genome encapsidation. Proc. Natl. Acad. Sci. USA *110*, 9048–9053.

Maclellan, K., Loney, C., Yeo, R.P., and Bhella, D. (2007). The 24-angstrom structure of respiratory syncytial virus nucleocapsid protein-RNA decameric rings. J. Virol. *81*, 9519–9524.

Marklewitz, M., Zirkel, F., Kurth, A., Drosten, C., and Junglen, S. (2015). Evolutionary and phenotypic analysis of live virus isolates suggests arthropod origin of a pathogenic RNA virus family. Proc. Natl. Acad. Sci. USA *112*, 7536–7541.

Marsh, J.A., and Teichmann, S.A. (2015). Structure, dynamics, assembly, and evolution of protein complexes. Annu. Rev. Biochem. *84*, 551–575.

Mazza, C., Ohno, M., Segref, A., Mattaj, I.W., and Cusack, S. (2001). Crystal structure of the human nuclear cap binding complex. Mol. Cell *8*, 383–396.

Niu, F., Shaw, N., Wang, Y.E., Jiao, L., Ding, W., Li, X., Zhu, P., Upur, H., Ouyang, S., Cheng, G., and Liu, Z.J. (2013). Structure of the Leanyer orthobunyavirus nucleoprotein-RNA complex reveals unique architecture for RNA encapsidation. Proc. Natl. Acad. Sci. USA *110*, 9054–9059.

Olal, D., Dick, A., Woods, V.L., Jr., Liu, T., Li, S., Devignot, S., Weber, F., Saphire, E.O., and Daumke, O. (2014). Structural insights into RNA encapsidation and helical assembly of the Toscana virus nucleoprotein. Nucleic Acids Res. *42*, 6025–6037.

Raymond, D.D., Piper, M.E., Gerrard, S.R., Skiniotis, G., and Smith, J.L. (2012). Phleboviruses encapsidate their genomes by sequestering RNA bases. Proc. Natl. Acad. Sci. USA *109*, 19208–19213.

Reguera, J., Malet, H., Weber, F., and Cusack, S. (2013). Structural basis for encapsidation of genomic RNA by La Crosse Orthobunyavirus nucleoprotein. Proc. Natl. Acad. Sci. USA *110*, 7246–7251.

Schmaljohn, C.S. (1995). The Molecular Biology of Hantaviruses (Springer).

Severson, W.E., Xu, X., and Jonsson, C.B. (2001). cis-Acting signals in encapsidation of Hantaan virus S-segment viral genomic RNA by its N protein. J. Virol. *75*, 2646–2652.

Tawar, R.G., Duquerroy, S., Vonrhein, C., Varela, P.F., Damier-Piolle, L., Castagné, N., MacLellan, K., Bedouelle, H., Bricogne, G., Bhella, D., et al. (2009). Crystal structure of a nucleocapsid-like nucleoprotein-RNA complex of respiratory syncytial virus. Science *326*, 1279–1283.

Taylor, S.L., Frias-Staheli, N., García-Sastre, A., and Schmaljohn, C.S. (2009). Hantaan virus nucleocapsid protein binds to importin alpha proteins and inhibits tumor necrosis factor alpha-induced activation of nuclear factor kappa B. J. Virol. *83*, 1271–1279.

Xu, X., Severson, W., Villegas, N., Schmaljohn, C.S., and Jonsson, C.B. (2002). The RNA binding domain of the hantaan virus N protein maps to a central, conserved region. J. Virol. *76*, 3301–3308.

Yoshimatsu, K., Lee, B.H., Araki, K., Morimatsu, M., Ogino, M., Ebihara, H., and Arikawa, J. (2003). The multimerization of hantavirus nucleocapsid protein depends on type-specific epitopes. J. Virol. *77*, 943–952.